BIOCHEMISTRY
including biophysical chemistry & molecular biology

Article

pubs.acs.org/biochemistry

The Maize (*Zea mays* L.) *Nucleoside Diphosphate Kinase1 (ZmNDPK1)* Gene Encodes a Human NM23-H2 Homologue That Binds and Stabilizes G-Quadruplex DNA

Mykhailo Kopylov,[†,‡] Hank W. Bass,[†] and M. Elizabeth Stroupe*[,†,‡]

[†]Department of Biological Science and [‡]Institute of Molecular Biophysics, Florida State University, 91 Chieftan Way, Tallahassee, Florida 32306-4380, United States

Supporting Information

ABSTRACT: Noncanonical forms of DNA like the guanine quadruplex (G4) play important roles in regulating transcription and translation through interactions with their protein partners. Although potential G4 elements have been identified in or near genes from species diverse as bacteria, mammals, and plants, little is known about how they might function as *cis*-regulatory elements or as binding sites for *trans*-acting protein partners. In fact, until now no G4 binding partners have been identified in the plant kingdom. Here, we report on the cloning and characterization of the first plant-kingdom gene known to encode a G4-binding protein, maize (*Zea mays* L.) *nucleoside diphosphate kinase1 (ZmNDPK1)*. Structural characterization by X-ray crystallography reveals that it is a homohexamer, akin to other known NDPKs like the human homologue NM23-H2. Further probing into the G4-binding properties of both NDPK homologues suggests that ZmNDPK1 possesses properties distinct from that of NM23-H2, which is known to interact with a G-rich sequence element upstream of the *c-myc* gene and, in doing so, modulate its expression. Indeed, ZmNDPK1 binds the folded G4 with low nanomolar affinity but corresponding unfolded G-rich DNA more weakly, whereas NM23-H2 binds both folded and unfolded G4 with low nanomolar affinities; nonetheless, both homologues appear to stabilize folded DNAs whether they were prefolded or not. We also demonstrate that the G4-binding activity of ZmNDPK1 is independent of nucleotide binding and kinase activity, suggesting that the G4-binding region and the enzyme active sites are separate. Together, these findings establish a broad evolutionary conservation of some NDPKs as G4-DNA binding enzymes, but with potentially distinct biochemical properties that may reflect divergent evolution or species-specific deployment of these elements in gene regulatory processes.

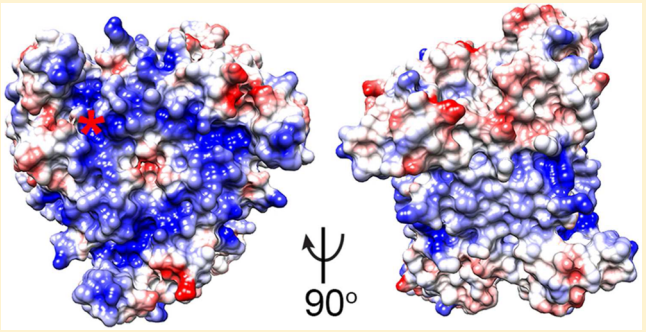

Guanine quartets occur when four guanines in a single-stranded DNA or RNA form Hoogsteen base pairs with one another, surrounding a central monovalent cation that is typically a potassium ion.[1] Sequential quartets can stack, forming an extended secondary structure where loops of single-stranded nucleic acid connect the quadruplexed guanines in a variety of topologies.[2,3] *In vivo*, these G-quadruplex (G4) motifs occur in G-rich regions of DNA, such as those found on the 3′-terminal strand in the telomeres of linear chromosomes.[4,5] Additionally, a preponderance of G4 motifs are found at genes, in particular at promoter regions, the 5′ ends of first introns, and 5′ and 3′ untranslated regions (UTRs) of some mRNAs, as well as in the long terminal repeats (LTRs) of some classes of plant retrotransposons.[6−11] G4 elements are implicated in DNA replication, telomere metabolism, and genome rearrangements; evidence for the specific involvement of DNA G4 structures, whose presence is affected by protein binding partners, in regulating these activities comes from nuclear staining of G4s and in functional disruption of both DNA and protein elements.[7,12] Further, *Escherichia coli* G4s encoded in the antisense strand at promoters result in decreased gene expression, whereas G4s encoded in the antisense strand of 5′UTRs result in enhanced gene expression.[13] Together, these discoveries reveal a remarkably broad and diverse deployment of G4s in nature, promoting the experimentally supported hypothesis that G4s participate in control of gene expression, including transcriptional initiation, splice site selection, or protein translation.[14−16]

G4 formation by short, G-rich oligonucleotides *in vitro* is strongly stabilized[17] by the addition of K^+.[18] *In vivo*, formation and function of G4s are likely influenced by *trans*-acting protein factors that stabilize or destabilize the G4 secondary structure, identified so far in *Archaea*, yeast, and metazoan species.[12,15,19−23] Early on, Puf transcription factor was identified as binding the G-rich region of DNA that is upstream of the *c-myc* promoter.[24] More recently, a number of G4 binding proteins have been identified that have diverse functions, illustrated by, but not limited to, xeroderma pigmentosum B

Received: October 13, 2014
Revised: February 10, 2015
Published: February 13, 2015

DOI: 10.1021/bi501284g
Biochemistry 2015, 54, 1743−1757

Table 1

G4 variant name	Sequence	Ability to form G4 ?	Compete for binding?
hexokinase4 antisense 5'UTR hex4 _A5U	CGGGGGTGTTGAAGGGAGGAGGAGGGAGGGG	YES	++++
hexokinase4 antisense intron1 hex4_A5I	TGGGGTGGGGGGGGAGCGGG	YES	+
hexokinase4 sense AUG (RNA) hex4_AUG	CGGGGGGAUGGGGCGGGUCGGG	YES	++
hexokinase4 antisense 5'UTR point mutant hex4_A5Um	CGacGGTGTTGAAGcGAGGAGGAGcGAGcGG	NO	+
double stranded *hexokinase4* antisense 5'UTR hex4_A5Uds	CGGGGGTGTTGAAGGGAGGAGGAGGGAGGGG GCCCCCACAACTTCCCTCCTCCTCCCTCCCC	NO	+
c-myc nuclease hypersensitive element III1 Pu44[53]	CGCTTATGGGGAGGGTGGGGAGGGTGGGGAAGGTGGGGAGGAGA	YES	not tested
c-myc nuclease hypersensitive element III1 Pu27[53]	TGGGGAGGGTGGGGAGGGTGGGGAAGG	YES	++
poly-adenine mutant PA	AAAAGAAAAAAAAGAAAAAAAAGAAAA	NO	-
c-myc nuclease hypersensitive element III1 point mutant Pu27m	TGGcGAGcGTGGcGAGcGTGGcGAAGG	YES	-
hex4_A5U loop 1 MS2-stemloop MS2_A5U1	CGTACACCTGTTGGTGTACG	NO	-
hex4_A5U loop 2 MS2-stemloop MS2_A5U2	CGTACACCTGAAGGTGTACG	NO	+
hex4_A5U loop 3 MS2-stemloop MS2_A5U3	CGTACACCGGAGGGTGTACG	NO	-

(XPB) and xeroderma pigmentosum D (XPD) helicases;[12] hnRNP A1 and its derivative unwinding protein 1 (Up1)[25] and the telomeric binding proteins protection of telomere-1 (POT1)[22] and repressor-activator protein 1 (RAP1).[26] No universal mechanism for G4 modulation by protein partners has emerged, perhaps because each protein−nucleic acid binding partner pair is unique but also suggesting more work needs to be done to fully define how G4 elements and their protein binding partners interact. Additionally, studies to date on genic G4 binding protein partners are primarily limited to bacteria, *Archaea*, yeast, and metazoan species, leaving open the question we address here: do members of the plant kingdom have protein partners that interact with their predicted genic G4s?

An emerging idea is that nucleoside diphosphate kinase (NDPK, EC 2.7.4.6) serves as a master regulator of diverse pathways in the cell because of its ubiquitous occurrence, whereas once it was thought to be only responsible for maintaining the nucleotide triphosphate pool throughout the cell, including within organelles. Surprisingly, after being recognized as important in *c-myc* expression, the Puf transcription factor was subsequently identified as NM23-H2, a member of the nonmetastatic 23 (NM23) family that binds to the G-rich *c-myc* nuclease hypersensitive element III_1.[27] The 10 members of the human NM23 family are defined by sequence conservation and can be divided into two groups based on whether or not they exhibit kinase activity.[28] Those that are kinases possess the characteristic residues that drive the enzyme's double-displacement (ping-pong) catalytic mechanism first described for the yeast NDPK.[29] A wide range of characteristics has been attributed to NDPK proteins in addition to trans-phosphorylation of nucleoside diphosphates, supporting the hypothesis that these enzymes serve a broader regulatory role in the cell. For example, NDPK has been found to bind G-rich single-stranded oligonucleotides;[30] oligomerize upon binding GTP to form microtubule-like bundles;[31] act as a protein histidine kinase;[32] activate GTPases;[33] or alter membrane dynamics by providing a steady stream of GTP to the dynamin molecular motors.[34,35] Additional functions for NDPKs in cell proliferation, signaling, and development are well documented for both fungal and animal species.[28,36] Plant NDPKs are known to facilitate analogous housekeeping and regulatory cellular functions, as well as playing a role in abiotic stress response,[17,37−43] but their DNA binding properties have not been described.

The locations of G4 sequence motifs in the maize genome were recently identified computationally, and these G4 motifs are enriched at promoters and introns of thousands of genes, many of which are coupled to energy stress signaling.[11] To understand the potential roles of these elements in this major crop and model plant species, we undertook an unbiased ligand-binding screen to identify proteins that interact with maize G4-forming sequences. From this screen, we identified maize cDNA clones for a gene encoding ZmNDPK1, representing the first biochemically defined G4-binding protein from plants. Here, we biochemically and structurally characterized ZmNDPK1 and its G4 interactions with comparative analysis of its human homologue, NM23-H2, allowing us to propose a model for NDPK interactions with G4 structures.

EXPERIMENTAL PROCEDURES

Phage Library Screen. A library of maize cDNAs was previously generated from meiosis-enriched tassels (library 11, inbred line W23, a gift from J. M. Gardiner, University of Arizona, Tucson) and clonded in the Lambda Zap II expression vector (Agilent Technologies, Santa Clara, CA). Phage λ

DOI: 10.1021/bi501284g
Biochemistry 2015, 54, 1743−1757

harboring this library were subsequently infected into Y1090a *Escherichia coli* for protein expression and ligand-binding screening according to the published method.[44] Plaques were lifted onto nitrocellulose, and then the membranes were blocked using 5% bovine serum albumin fraction V (BSA), 50 mM Tris·HCl (pH 7.4), 50 mM NaCl, 1 mM EDTA·NaOH (pH 8), and 1 mM DTT. To reduce detection of endogenous nonspecific biotinylation from the *E. coli* host, the membranes were next blocked with 2 μg/mL avidin in 12 mM potassium/sodium phosphate (pH 7), 137 mM NaCl, 2.7 mM KCl, and 0.05% Tween-20 (PBST), washed in PBST, and blocked again in 100 nM biotin in PBST. 60 nM biotinylated G4 folded oligonucleotide from the antisense strand of the 5′ UTR of the maize *hexokinase4* gene (the oligonucleotide is hereafter called *hex4*_A5U - "A5U" for antisense 5′ UTR; Figure S1 and Table 1) in 10 mM Tris·HCl (pH 7.4), 10 mM KCl, and 40 mM NaCl was applied and then washed with the same buffer minus probe. All G4 or G4 mutant oligonucleotides were annealed according to the same procedure: oligonucleotides were mixed in KCl- or LiCl-containing buffers, as designated, heated to 95 °C for 15 min, and cooled to room temperature overnight. The G4 state for all was verified with thermal difference spectroscopy (TDS, Figure S1, Supporting Information and Table 1). Membranes were cross-linked in a Stratalinker 1800 (Agilent, Santa Clara, CA), and the oligonucleotide-binding plaques were identified by detection of biotin with NeutrAvidin-conjugated horseradish peroxidase (HRP, Thermo Scientific, Rockford, IL), developed with chloronaphthol- and diaminobenzidine-based (CN/DAB) colorimetric stain (Thermo Scientific, Rockford, IL). Initial hits were plaque purified, and the ZmNDPK1 gene was identified from three independent clones using polymerase chain reaction (PCR) with M13 primers followed by sequencing of the PCR product. A full-length cDNA clone for the ZmNDPK1 gene (GenBank accession number KM347972) was used as a template for PCR amplification using sequence-specific primers (complementary regions are underlined, forward: GCTTAGCATATGGAGAGCACCTTCATC and reverse: CTTATCGAATCCTTACTTCTCGTAGATCCAGG), and the PCR product was subsequently subcloned into the pET28a (EMD Millipore, Darmstadt, Germany) vector as a hexa-histidine (his-tag) fusion. The resulting N-terminal six histidine tagged fusion protein was used for this study. All oligonucleotides for G4 studies and cloning were purchased from Eurofins Genomics, Huntsville, AL.

Protein Expression and Purification. BL21(DE3) *E. coli* cells were transformed with ZmNDPK1 pET28a or NM23-H2 pET28a, and cells were grown to an A_{600} of 0.4−0.6 at 37 °C before induction with 0.5 mM IPTG for overnight expression. The protein purification for both homologues was identical. Cells were harvested and resuspended in 50 mM sodium HEPES (pH 7.5) and 100 mM KCl buffer (buffer A) before being lysed with a microfluidizer. Lysate was clarified through centrifugation at 16000*g* for 30 min at 4 °C in an Eppendorf F-34-6-38 fixed angle rotor (Hamburg, Germany). Clarified lysate was then passed over nickel-nitrilotriacetic acid (NTA) (GE Healthcare, Piscataway, NJ), washed in 50 mM imidazole +buffer A, washed in 50 mM imidazole + buffer A + 1 M KCl, re-equilibrated into 50 mM imidazole + buffer A and then recovered by imidazole gradient elution around 400 mM imidazole. Eluate was dialyzed against buffer A before being concentrated for size exclusion chromatography over a Sephacryl S100 column (GE Healthcare, Piscataway, NJ). All protein concentrations were determined by the absorbance at A_{280} using the BCA-determined extinction coefficient and expressed in terms of the concentration of the monomer.

Point Variant Generation and Purification. H115A and K149A point mutants were generated in the ZmNDPK1 expression construct using the following QuikChange (Agilent Technologies, Santa Clara, CA) primers, where the variant codons are in italics (H115A: CATTGGCAGGAATGTCATT*GCT*GGAAGTGACAGCATTGAGAGTGC plus reverse complement; K149A: CCCTGGATCTACGAG*GCG*TAAGGATTCGATCGAGCTCCGTCG plus reverse complement). Proteins were expressed and purified as described above for the wild-type proteins.

Structure Determination. ZmNDPK1 crystals were initially identified from the Hampton Crystal Screen 1 condition 40 (Hampton Research, Aliso Viejo, CA) and subsequently refined to 100 mM sodium cacodylate (pH 6.5), 12% PEG 8000, and 200 mM $CaCl_2$. Crystals were washed in 20% PEG 8000 before flash freezing in liquid nitrogen. X-ray diffraction data to 2.0-Å resolution were collected on Beamline 22-BM at the Advanced Photon Source within Argonne National Laboratories (Argonne, IL). Data were indexed and reduced in HKL2000.[45] Phases were determined using molecular replacement in PHENIX[46] against an all alanine model of AtNDPK1 (modified from PDB ID 1U8W[47]), and the structure was refined with simulated annealing and energy minimization in Phenix.[46]

Maize Extract Pulldown. Seeds from the B73 cultivar of *Z. mays* were ground in a coffee grinder. Seed powder was hydrated in buffer B (25 mM sodium HEPES (pH 7.5), 25 mM NaCl, 100 mM KCl, 4.5 mM $MgCl_2$, 5 mM EDTA, 10% weight/volume glycerol, 0.2 mM PMSF, and 0.02% protease inhibitor cocktail (Sigma-Aldrich, St. Louis, MO)) and extracted in a dounce homogenizer. Solids were removed with centrifugation and the extract was separated with heparin affinity chromatography. ZmNDPK1-containing fractions were identified with Western blot analysis using a new ZmNDPK1-specific antibody (Figure S2). Magnetic Dynabeads MyOne Streptavidin C1 beads (Life Technologies, Carlsbad CA) were prepared by blocking with buffer A plus 0.5% BSA and 10 μg/mL heparin (Alfa Aesar, Ward Hill, MA) before addition of biotinylated G4 folded *hex4*_A5U or biotinylated unfoldable *hex4*_A5Um sequences (Figure S1 and Table 1) with an additional 30 nt linker to biotin. ZmNDPK1-containing fractions from the heparin affinity separation were mixed with the oligonucleotide-bound beads and incubated for 1 h at 4 °C with rotation. Bound proteins were washed with buffer B and eluted in buffer B + 1 M KCl. Proteins were separated by SDS-PAGE, transferred to nitrocellulose membrane, and analyzed with the same ZmNDPK1-specific antibody.

K_d and Stoichiometry Determination. We determined the apparent binding affinity of Zm-NDPK1 for folded *hex4*_A5U using a modified slot-blot binding assay.[48−50] Probe, 0.1 nM biotinylated G4 folded *hex4*_A5U DNA (Figure S1 and Table 1), was mixed at 22 °C with increasing ZmNDPK1 protein concentrations from 0 to 55 nM in buffer C (10 mM sodium HEPES (pH 7.5) and 20 mM KCl supplemented with 10 μg/mL heparin). The mixture was then applied to a slot blot apparatus that passed the solution through stacked Hybond-C Extra nitrocellulose, 0.45 μm pore size (GE Healthcare Life Sciences, Piscataway, NJ) and negatively charged Nytran N nylon (GE Healthcare Life Sciences, Piscataway, NJ) membranes via capillary action. The binding

DOI: 10.1021/bi501284g
Biochemistry 2015, 54, 1743−1757

experiments were designed to show specificity, within the salt tolerance of the experiment: increasing salt causes nonspecific nucleic acid binding to nitrocellulose.[51] Notably, addition of up to 1000-fold excess random ssDNA in addition to the heparin did not affect the shift of the oligonucleotide to nitrocellulose, although it did quench the biotin signal on the nylon membrane (data not shown). At 0.1 nM oligonucleotide, no DNA binds nitrocellulose but is retained on nitrocellulose in the presence of increasing amounts of protein (Figure S3). Both membranes were UV-cross-linked before blocking. Nitrocellulose membranes were blocked for 1 h in 2% BSA in 50 mM Tris (pH 7.4) and 150 mM NaCl (TBS), whereas nylon membranes were blocked in 4% dry milk in TBS. The presence of biotinylated oligonucleotide was detected with NeutrAvidin-conjugated HRP (Thermo Scientific, Rockford, IL) that was developed with CN/DAB colorimetric stain (Thermo Scientific, Rockford, IL). Membranes were scanned on a flatbed scanner and the integrated intensities of the slots were determined in ImageJ.[52] This protocol was followed for ZmNDPK1 and biotinylated *hex4*_A5U in buffer C with LiCl rather than KCl, spanning protein concentrations of 0 to 2200 nM. Slot blots were repeated with NM23-H2 and biotinylated Pu44, the well-characterized human G4 element[53] (Figure S1 and Table 1), in buffer C with KCl or LiCl, spanning protein concentrations of 0 to 18 nM for both. We also performed the experiments titrating ZmNDPK1 from 0 to 2000 nM against biotinylated Pu44 in KCl or LiCl and NM23-H2 from 0 to 500 nM against biotinylated *hex4*_A5U in KCl or LiCl. We then titrated ZmNDPK1 point variants against biotinylated *hex4*_A5U. H115A spanned the concentration range 0 to 250 nM in KCl and 0 to 2000 nM in LiCl. K149A spanned the concentration range 0−2000 nM in both KCl and LiCl.

The K_d was calculated by fitting the modified Hill equation, eq 1, to three independently determined plots of increasing protein concentration against the fraction of protein-bound DNA using an in house Python script (Enthought, Austin, TX). In eq 1, P_t is the protein concentration in terms of monomers, calculated from its A_{280} and experimentally determined extinction coefficient, and h is the Hill coefficient (Table 2).

$$\text{fraction bound} = \frac{1}{1 + \left(\frac{K_d}{[P_t]}\right)^h} \quad (1)$$

The stoichiometry of binding was determined by titrating protein against 5 or 10 nM biotinylated G4 folded *hex4*_A5U in buffer C. Cross-linking, blocking, and detection was performed as described above.

Table 2

NDPK homologue	oligonuclotide (salt)	K_d(nM)	h
ZmNDPK1	hex4_A5U (KCl)	6.8 ± 0.3	2.1 ± 0.1
ZmNDPK1	hex4_A5U (LiCl)	289 ± 1	4.0 ± 0.1
NM23-H2	Pu44 (KCl)	1.2 ± 0.2	2.0 ± 0.2
NM23-H2	Pu44 (LiCl)	1.6 ± 0.1	1.7 ± 0.2
ZmNDPK1	Pu44 (KCl)	91 ± 13	1.0 ± 0.1
ZmNDPKI	Pu44 (LiCl)	476 ± 44	3.9 ± 0.7
NM23-H2	hex4_A5U (KCl)	33 ± 2	1.6 ± 0.1
NM23-H2	hex4_A5U (LiCl)	24 ± 1	2.1 ± 0.1
ZmNDPK1 H115A	hex4_A5U (KCl)	6.9 ± 0.7	1.8 ± 0.1
ZmNDPK1 H115A	hex4_A5U (LiCl)	287 ± 14	1.9 ± 0.1
ZmNDPKI K149A	hex4_A5U (KCl)	31 ± 2	1.6 ± 0.2
ZmNDPK1 K149A	hex4_A5U (LiCl)	>2000	N/A

Competition Experiments. Biotinylated G4 folded *hex4*_A5U at 1 nM was mixed with KCl-annealed competitor (Figure S1 and Table 1) at 1-, 10-, and 100-fold molar excess competitor over biotinylated probe and then 3 nM ZmNDPK1 was added. The mixture was incubated for 15 or 60 min before being applied to the slot blot apparatus. Each competitor oligonucleotide was treated in the same way. Nitrocellulose retention was measured in triplicate using the NeutrAvidin/CN/DAB protocol described above. Percent retention was calculated against a zero competitor control. Nucleotide competition was performed in a similar way using identical protein and DNA concentrations but using 0−1 mM ATP, ADP, GTP, or GTPγS and 2.5 mM $MgCl_2$ in place of the competing oligonucleotide.

Activity Assays. The standard assay for this activity is an enzyme-coupled assay in which NDPK converts ATP + TDP to ADP + TTP. Pyruvate kinase (PK), in turn, transfers a phosphate from phosphoenolpyruvate (PEP) to ADP, regenerating ATP and making pyruvate. Finally, lactate dehydrogenase (LD) converts pyruvate and β-NADH to the spectroscopically inactive NAD^+, and this decrease in absorbance is monitored at 340 nm.[54] ZmNDPK's kinase activity was measured as free enzyme at 2.5 nM concentration or in the presence of saturating (250 nM) *hex4*_A5U either in the presence of 20 mM KCl or LiCl, that is, either with G4 folded or single-stranded G-rich oligonucleotide. Buffer conditions included 100 mM Tris-HCl (pH 7.5), 10 mM $MgCl_2$, 0.7 mM TDP, 6 mM ATP, 0.4 mM NADPH, 4 mM PEP, 10 U PK, and 10 U LD. Standard activities for wild type and point variant (H115A or K149A) ZmNDPK1 were measured in 100 mM KCl. Activities were measured in the kinetics mode of an Agilent 8453 spectrophotometer at 25 °C. Activity measurements of NM23-H2 were also made using the same assay as free enzyme and with G4 folded or single-stranded G-rich Pu27 oligonucleotide (a shortened form of Pu44,[53] Table 1).

G4 DNA Folding Experiments. Förster resonance energy transfer (FRET) probes were designed based on the *hex4*_A5U or Pu27 G4 oligonucleotide sequences (Table 1) but labeled 5′ with 6-carboxyfluorescein (6-FAM) and 3′ with carboxytetramethylrhodamine (TAMRA) (Eurofins Genomics, Huntsville, AL). Single label oligonucleotides were also generated as controls for FRET efficiency. Reactions were set up in triplicate in black 96-well Nunclon plates (Thermo Fisher Scientific), and each reaction contained 200 μL of 200 nM FRET probe in 10 mM tetrabutylammonium phosphate (TBA) buffer (pH 7.5) supplemented with either 20 mM KCl or LiCl. Protein was added at increasing concentrations from 100 to 900 nM (0.5−9-fold excess) and plates were incubated for 1 h at 4 °C before data collection. Data were collected on a Spectramax M5 multimode plate reader (Molecular Devices) using 475 nm excitation wavelength and 515 nm cutoff. Emission spectra were collected at 21 °C from 500 to 640 nm with 2 nm step and 10 reads per well. FRET efficiency was characterized by computing the parameter P,[55] which we refer to as P_F:

$$P_F = \frac{I_d}{I_d + I_a} \quad (2)$$

where I_d is the intensity of the FRET donor (FAM) at 520 nm and I_a is the intensity of the FRET acceptor (TAMRA) at 584 nm.

DOI: 10.1021/bi501284g
Biochemistry 2015, 54, 1743−1757

A.

```
ZmNDPK1    ------------------------------------------------------------
AtNDPK1    ------------------------------------------------------------
HsNM23-H2  ------------------------------------------------------------
AtNDPK2    MVGATVVSKWTPLCVASPPERNSASLNPHCSPARVNFRTALAAFRPQFRLFSRNSASRRR  60
AtNDPK3    -------------------------------------------MSSQICRSASKAAKS  15

ZmNDPK1    ----------------------MESTFIMIKPDGVQRGLIGEIISRFEKKGFYLKALKLV  38
AtNDPK1    --MCGLYINLFCLLRITSNKKTMEQTFIMIKPDGVQRGLIGEVICRFEKKGFTLKGLKLI  58
HsNM23-H2  -------------------MANLERTFIAIKPDGVQRGLVGEIIKRFEQKGFRLVAMKFL  41
AtNDPK2    LRASSSAESGIFLPHLVASMEDVEETYIMVKPDGIQRGLVGEIISRFEKKGFKLIGLKMF 120
AtNDPK3    LLSSAKNARFFSEGRAIGAAAAVSASGKIPLYASNQRGLISEIISRFERKGFKLVGIKVI  75
                                 :. :       . ****:.*:* ***:*** * .:*..

ZmNDPK1    NVERSFAEKHYADLASKPFFQGLVDYIISGPVVAMVWEGKSVVTTGRKIIGATNPLASEP  98
AtNDPK1    SVERSFAEKHYEDLSSKSFFSGLVDYIVSGPVVAMIWEGKNVVLTGRKIIGATNPAASEP 118
HsNM23-H2  RASEEHLKQHYIDLKDRPFFPGLVKYMNSGPVVAMVWEGLNVVKTGRVMLGETNPADSKP 101
AtNDPK2    QCPKELAEEHYKDLSAKSFFPNLIEYITSGPVVCMAWEGVGVVASARKLIGKTDPLQAEP 180
AtNDPK3    VPSKDFAQKHYHDLKERPFFNGLCDFLSSGPVIAMVWEGDGVIRYGRKLIGATDPQKSEP 135
              ..  ::** **  :.** .* .:: ****:.* *** .*:  .* ::* *:*  ::*

ZmNDPK1    GTIRGDFAVDIGRNVIHGSDSIESANKEIALWF-PEGLADWQSSQHPWIYEK- 149
AtNDPK1    GTIRGDFAIDIGRNVIHGSDSVESARKEIALWF-PDGPVNWQSSVHPWVYET- 169
HsNM23-H2  GTIRGDFCIQVGRNIIHGSDSVKSAEKEISLWFKPEELVDYKSCAHDWVYE-- 152
AtNDPK2    GTIRGDLAVQTGRNIVHGSDSPENGKREIGLWFKEGELCKWDSALATWLRE-- 231
AtNDPK3    GTIRGDLAVTVGRNIIHGSDGPETAKDEISLWFKPQELVSYTSNSEKWLYGDN 188
           ******:.:  ***::****. :... **.***      .: *    *:
```

B.

```
ZmNDPK1     100.00
AtNDPK1     82.55   100.00
HsNM23-H2   62.84    60.93   100.00
AtNDPK2     58.11    50.60    51.32   100.00
AtNDPK3     53.69    46.75    51.97    44.09   100.00
```

Figure 1. ZmNDPK1 is a canonical NDPK. (A) Sequence alignment by *Clustal Omega*[71] of ZmNDPK with three *A. thalina* (*At*) and the closest human (*Hs*) homologues shows the high homology of this conserved enzyme. Peptides at the C-terminus are the most strongly divergent, demarked by an underline showing the peptide used to raise the antibody against ZmNDPK1. Divergent aa's are in italics. The active site histidine is in bold. An asterisk (*) marks aa sequence identity, A colon (:) marks strong aa sequence similarity; a period (.) marks weak aa sequence similarity. The dark black line highlights the PFAM PF00334 NDPK domain. (B) The percent identity matrix shows the highest aa identity between ZmNDPK and AtANPK1.

RESULTS

The ZmNDPK1 Gene Encodes a Protein with G4-Binding Activity. ZmNDPK1 was identified from a G4 ligand-binding screen of a maize meiosis-enriched tassel cDNA phage expression library, modified from a dsDNA ligand screen.[44] A biotinylated oligonucleotide corresponding to a G4 motif (G4v2-53046)[11] from the antisense strand of the 5′ UTR of the maize *hexokinase4* gene (*hex4*_A5U) was prefolded in KCl into the G4 conformation and used as the ligand. Oligonucleotides and their names that were used in this study are given in Table 1. G4 formation was verified with thermal melt difference spectroscopy (TDS) (Figure S1) and shown to be K^+ (Figure S1A,B) and sequence (Figure S1C,D) specific. From approximately one million phage screened with a plaque lift filter binding assay, we purified several independent cDNA clones, each corresponding to a previously uncharacterized maize gene predicted to encode an NDPK domain (PFAM PF00334 and Figure 1). This gene is from one of at least nine loci in the maize genome that code for proteins with an NDPK domain. The predicted protein from our maize cultivar W23 full-length cDNA clone, GenBank accession number KM347972, is 149 amino acids (aa) in length, beginning with MES and ending with YEK and corresponding to transcript "T03" from gene model GRMZM2G178576 of the reference genome cultivar B73. Here we name this maize gene *nucleoside diphosphate kinase1, ZmNDPK1,* and its protein product as ZmNDPK1 (UniGene Zm.92368, with reference sequence: XP_008658458.1, Figure 1A). RNA from this locus is detected in many different maize tissues, with particularly high levels in developing and matured seed.[56] Compared to NDPKs from other eukaryotes, this clone shares 83% aa identity with *Arabidopsis thaliana* NDPK1 (AtNDPK1), 58% aa identity with AtNDPK2, 54% aa identity with AtNDPK3, and 63% aa identity with *Homo sapiens* NM23-H2 (Figure 1B). On the basis of this sequence identity pattern, we note that ZmNDPK1 has higher sequence identity to human NM23-H2 (also called NME2) than some other plant NDPKs (Figure 1). Further phylogenetic analysis of protein sequence similarity searches revealed that the NDPKs with a terminal lysine residue (referred to here by their three terminal amino acids, YEK) were found in several other grass species, all of which were in the *Panicoideae* subfamily of the *Poaceae* family of monocotyledonous (grass) plant species (Figure S4).

The full-length cDNA was subcloned into a bacterial overexpression vector (pET28a) to produce an N-terminal his-tagged fusion. We also generated the equivalent expression construct for NM23-H2. Both proteins overexpressed strongly and were purified by nickel affinity chromatography with a high salt wash to remove nonspecific DNA. Size exclusion chromatography further purified the protein to high homogeneity. Protein concentration of the purified protein was measured by the bicinchonic acid (BCA) colorometric assay

DOI: 10.1021/bi501284g
Biochemistry 2015, 54, 1743−1757

(Thermo Scientific, Rockford, IL), and the extinction coefficient at A_{280} was calculated to be 35 530 cm^{-1} M^{-1}. In this study, all concentrations are expressed in relation to the protein monomer concentration. Full-length, purified, recombinant ZmNDPK1 was stored in 50 mM HEPES (pH 7.5)/100 mM KCl and used for all subsequent experiments.

Structure Determination of ZmNDPK1. Crystals in the space group $P2_1$, with two hexamers in the asymmetric unit and a unit cell of 66.9 Å × 179.1 Å × 99.5 Å, diffracted to 2 Å resolution. The structure refined to an R_{free} of 20.1% and R_{work} of 16% (Table S1). ZmNDPK1 shares the general structural features of other hexameric NDPKs, including the active site histidine that participates in the transphosphorylation reaction (Figures 1 and 2). Indeed, ZmNDPK1 maintains its hexameric

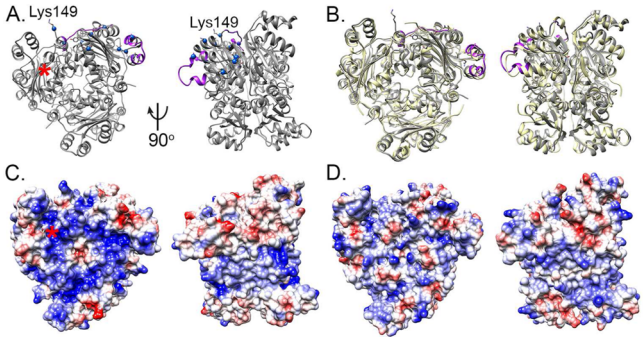

Figure 2. Hexameric NDPKs have high structural homology. (A) ZmNDPK1 is a canonical hexameric NDPK whose active site sits at a deep cleft, marked by a red asterisk (*). Three active sites are related by a 3-fold symmetry axis, which is perpendicular to the plane of the page. Turning the hexamer by 90° highlights the 2-fold symmetry axis. Blue balls demark the most divergent amino acids (italics in Figure 1). The active site loop and C-terminus, the most divergent regions of the structure, are highlighted in purple. Lys149 sits at the junction of the 3-fold and 2-fold axis. (B) ZmNDPK1 (gray) and NM23-H2 (yellow) are highly homologous. (C) The charged surface of ZmNDPK1 shows strongly basic regions (blue) at the active site cleft, marked by a red asterisk, and in a patch at the junction of the two- and 3-fold symmetry axis. (D) NM23-H2 does not show as strongly a charged surface as ZmNDPK1. Molecular graphics and analyses were performed with the UCSF Chimera package. Chimera is developed by the Resource for Biocomputing, Visualization, and Informatics at the University of California, San Francisco (supported by NIGMS P41-GM103311).[72]

assembly state even at 20 nM monomer concentration but can form dodecamers, as seen in the asymmetric unit, at higher concentrations (Figure S6). The known nucleotide binding active site is a long, positively charged cleft on the surface of the protein that lies between the core α/β fold and hairpin turn that connects α-helices 3 and 4 (Figure 2A,C). Despite strong sequence and structural conservation between this NDPK, two *Arabidopsis* homologues and one human homologue (Figure 1), ZmNDPK1 has an important and uniquely charged surface charge determined by specific amino acids throughout the protein, several of which have been previously shown to be important for DNA binding in NM23-H2[57] (Figure 2A,B). One of these nonconserved stretches localizes to the hairpin turn that contributes to the active site as well as to both the 3-fold and 2-fold faces of the hexamer, comprised of Ala53 to Phe57. The second nonconserved stretch creates a long loop that sits at the surface of the dimer interface, Pro132 to Lys149. This stretch ends at the C-terminal lysine (Lys149), which is unique to ZmNDPK1 and contributes to a positively charged patch at the edge of the trimer and dimer faces (Figure 2).

The divergent hairpin forms the upper wall of the active site cleft, sitting at the edge of the trimer and dimer interfaces (Figure 2A). Interestingly, this hairpin also forms one interface between successive hexamers in the dodecamer (Figure S5B). Consequently, the loop of the divergent hairpin in the interface subunit shows the only structural divergence from the common hexameric NDPK structure shared by NM23-H2, ZmNDPK1, and other eukaryotic NDPKs. Specifically, when the monomer subunits are superimposed, the average root-mean-square distance (RMSD) between the 145 Cαs of the 11 most similar subunits is 0.3 ± 0.1 Å, whereas the 11 Lys55 Cαs from the same 11 subunits are within 0.4 ± 0.2 Å of one another. In contrast, the average RMSD for the 145 Cαs of the subunit that contains the divergent active site loop aligned to the other 11 subunits is 0.5 ± 0.04 Å but Lys55 Cα from the divergent loop is 2.8 ± 0.3 Å away from the other Lys55 Cαs.

Native and Recombinant ZmNDPK1 Bind to G4 Element hex4_A5U. To confirm that the interaction between *hex4*_A5U and ZmNDPK1 also occurs with native ZmNDPK1 from maize, we mixed biotinylated, folded *hex4*_A5U oligonucleotide or a biotinylated unfoldable mutant *hex4*_A5Um (Figure S1 and Table 1) with heparin-fractionated maize seed extract and precipitated the proteins that interact with either oligonucleotide. A Western blot probed with an antibody raised against a unique ZmNDPK1 peptide (Figures 1 and S2) showed that native, endogenous ZmNDPK1 coprecipitates with the folded *hex4*_A5U oligonucleotide but not the unfoldable mutant (Figure 3).

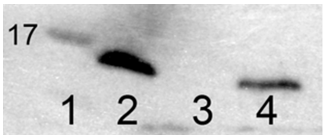

Figure 3. *hex4*_A5U binds to native ZmNDPK1. Western blotting using a specific ZmNDPK1 antibody against recovered proteins from a maize seed-extract pulldown show that native ZmNDPK1 does not bind an unfoldable form of *hex4*_A5U (*hex4*_A5Um) but does bind folded *hex4*_A5U. Lane 1:17 kDa marker. Lane 2: ZmNDPK1-containing fraction from heparin separated maize seed extract (input). Lane 3: elution from pulldown using unfoldable *hex*_A5Um. Lane 4: elution from pulldown using folded *hex4*_A5U.

ZmNDPK1 and NM23-H2 Have Different G4 Binding Properties. Given the qualitative similarities between the ZmNDPK1 and NM23-H2, we compared the binding properties of the homologues using a straightforward slot blot binding assay. First, we folded either *hex4*_A5U or Pu44[53] oligonucleotide by heating and slow annealing in the presence of 20 mM KCl (Figure S1A and Table 1). Second, we measured the retention of the protein:DNA complexes (either ZmNDPK1:*hex4*_A5U or NM23-H2:Pu44) on nitrocellulose and the binding of free DNA to nylon through a slot apparatus using detection of DNA-coupled biotin (Figure S3). Under these conditions, ZmNDPK1 bound prefolded *hex4*_A5U with an apparent K_d of 6.8 ± 0.3 nM and a Hill coefficient of 2.1 ± 0.1 whereas NM23-H2 bound prefolded Pu44 with an apparent K_d of 1.1 ± 0.1 nM and a Hill coefficient of 2.0 ± 0.2 (Figure 4A,B, Table 2).

Next, we characterized ZmNDPK1 or NM23-H2 binding to its cognate oligonucleotide when the DNA is heated and

DOI: 10.1021/bi501284g
Biochemistry 2015, 54, 1743−1757

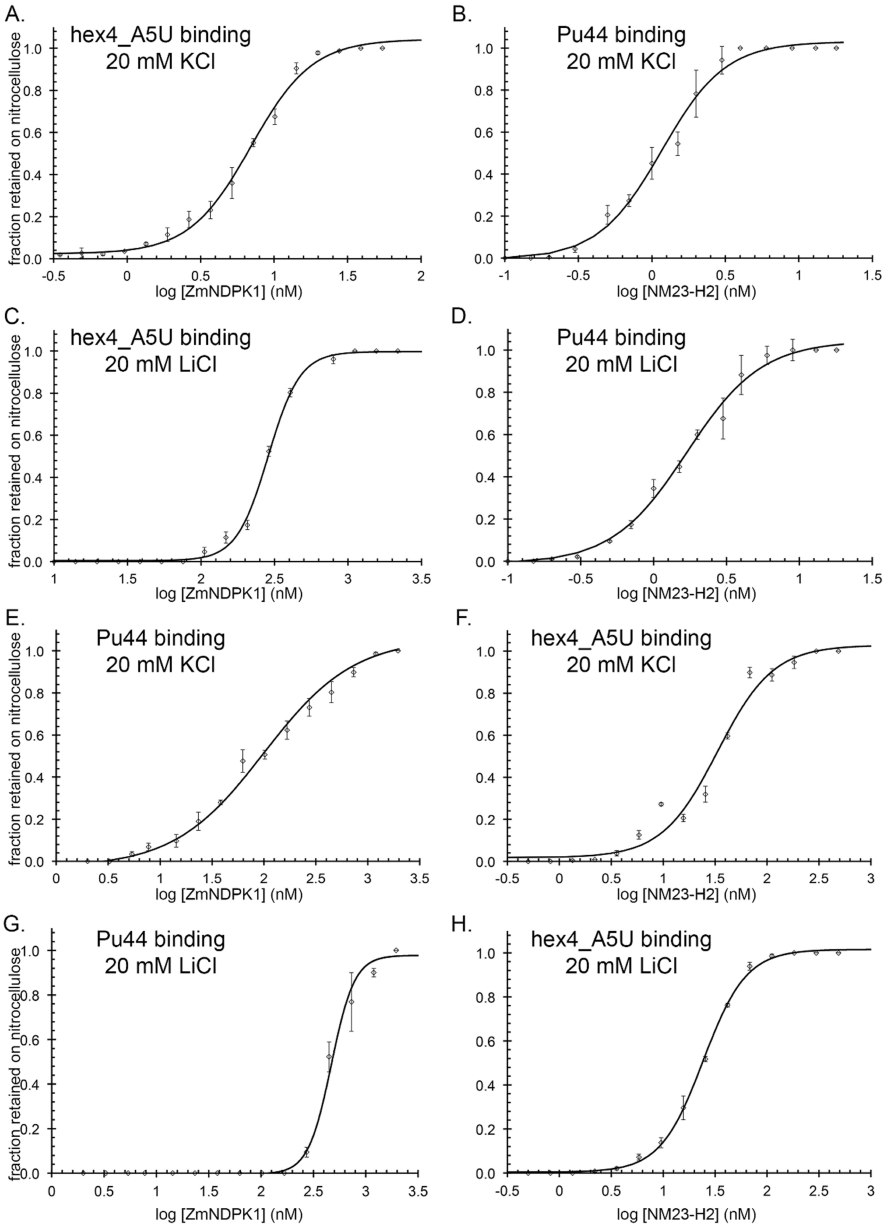

Figure 4. ZmNDPK1 and NM23-H2 bind folded G4 oligonucleotides with nM affinity. Increasing protein concentration increases the fraction of oligonucleotide that is retained on the nitrocellulose. (A) *hex4*_A5U oligonucleotide titration with ZmNDPK1 in 20 mM KCl. (B) Pu44 oligonucleotide titration with NM23-H2 in 20 mM KCl. **C.** *hex4*_A5U oligonucleotide titration with ZmNDPK1 in 20 mM LiCl. (D) Pu44 oligonucleotide titration with NM23-H2 in 20 mM LiCl. (E) Pu44 oligonucleotide titration with ZmNDPK1 in 20 mM KCl. (F) *hex4*_A5U oligonucleotide titration with NM23-H2 in 20 mM KCl. (G) Pu44 oligonucleotide titration with ZmNDPK1 in 20 mM LiCl. (H) *hex4*_A5U oligonucleotide titration with NM23-H2 in 20 mM LiCl.

annealed in the presence of Li^+, which does not support G4 formation (Figure S1B). ZmNDPK1 bound unfolded *hex4*_A5U with an apparent K_d of 288 ± 1 nM and Hill coefficient of 4.0 ± 0.1, whereas NM23-H2 bound Pu44 with an apparent K_d of 1.6 ± 0.1 nM and Hill coefficient of 0.7 ± 0.2 (Figure 4C,D and Table 2). These observations reveal an important and unexpected difference between the G4-binding activity of maize and human NDPK: ZmNDPK1 binds 40-fold more strongly to prefolded than unfolded G4 DNA whereas NM23-H2 binds to both prefolded and unfolded G4 DNA with similar affinity.

Finally, we asked whether the difference in G4 binding by the maize and human NDPKs arose from the protein homologue or from the G4 DNA (Figure 1 and Table 1). To answer our question, we performed reciprocal binding titrations, i. e., ZmNDPK1 against Pu44 and NM23-H2 against *hex4*_A5U, using the same slot blot assay. We calculated that ZmNDPK1 binds prefolded Pu44 G4 DNA (in KCl) with an apparent K_d of 91 ± 13 nM and a Hill coefficient of 1.0 ± 0.1 but binds unfolded Pu44 G4 DNA (in LiCl) with an apparent K_d of 476 ± 44 nM and a Hill coefficient of 3.9 ± 0.7. In contrast, NM23-H2 binds prefolded *hex4*_A5U G4 DNA (in KCl) with an apparent K_d of 33 ± 2 nM and a Hill coefficient of 1.6 ± 0.1 but binds unfolded *hex4*_A5U G4 DNA (in LiCl) with an apparent K_d of 24 ± 1 nM and a Hill coefficient of 2.1 ± 0.1.

ZmNDPK1 Binding to G4 DNA Is Specific and They Bind with Defined Stoichiometry. We further tested ZmNDPK1 binding preference using a panel of nucleotide

DOI: 10.1021/bi501284g
Biochemistry 2015, 54, 1743−1757

variants to compete for *hex4*_A5U binding (Table 1 and Figures S1 and S7). The unbiotinylated *hex4*_A5U oligonucleotide was the only DNA sequence tested that competed for binding at 10-fold excess and completely at 100-fold excess whether incubated for 15 or 60 min (Figure S7A,D). Two other G4-capable oligonucleotides, Pu27[53] and the RNA G4 *hex4*_AUG (a genic, sense-stranded G4 from the *hexokinase4* gene[11]), competed less efficiently than *hex4*_A5U, suggesting that ZmNDPK1 possesses some general G4 binding ability. Specifically, at 15 min *hex4*_AUG competed with about 50% efficiency at 100-fold excess and Pu27 with about 75% efficiency at 100-fold excess (Figure S7B). After 60 min, *hex4*_AUG competed with about 75% efficiency at 10-fold excess but never completely, even at 100-fold excess (Figure S7E). That these oligonucleotides behaved differently after different time points suggests that the system was not at equilibrium at 15 min and may not be at 60 min. Lower competition by Pu27 compared to *hex4*_A5U is consistent with the 5-fold weaker binding of ZmNDPK1 to the related Pu44 oligonucleotide (Figure 4 and Table 2). The RNA *hex4*_AUG oligonucleotide folds into a G4 even without KCl (Figure S1C), which is expected because RNA quadruplexes are more stable than DNA quadruplexes.[58−61]

Similarly, the G4-capable oligonucleotide *hex4*_A5I (another genic G4 from the *hexokinase4* gene[11]), *hex4*_A5Uds, *hex4*_A5Um, and MS2_A5U2 partially competed only at 100-fold excess after 60 min incubation but not after 15 min incubation, suggesting either nonspecific oligonucleotide binding or weak binding of the single-stranded molecule (Figure S7). Unfoldable single-stranded mutants (Pu27m or PA) and two stem loop mimics (MS2_A5U1 or MS2_A5U3) did not compete, even at 100-fold excess, under either incubation scheme (Figure S7C,F).

Finally, the binding stoichiometry was determined by titrating the protein against saturating G4-folded oligonucleotide. The resulting binding titration showed that one *hex4*_A5U bound to three ZmNDPK1 monomers (Figure S5), suggesting that if ZmNDPK1 is a hexamer, two G4s bind per hexamer.

ZmNDPK1 G4 Binding, Nucleotide Binding, and Nucleoside Kinase Activity. A specific model for G4 binding has already been suggested to explain binding of NM23-H2 for the unfolded, G-rich *c-myc* nuclease hypersensitive element III_1, predicting that the tandem Gs bind sequentially to the three nucleotide binding sites on the trimer face.[53] Additional amino acids previously shown to be important for NM23-H2 binding DNA are on the 2-fold symmetry face of the hexamer,[57] however, supporting an alternative model that predicts oligonucleotide binding around the edge of the two faces of the protein.[62] The more recent model that places the G-rich oligonucleotide binding at the active sites[53] leads to the prediction that saturating nucleotide (nucleotides bind with 10−20 μM affinity[63]) would sterically compete for oligonucleotide binding. To test this steric hindrance prediction, we examined equilibrium binding of ZmNDPK1 for *hex4*_A5U in the presence several nucleotides (Figure 5). Up to 1 mM ATP, ADP, GTP, or GTPγS failed to block G4 *hex4*_A5U binding to ZmNDPK1. Rather, GTPγS may slightly strengthen the interaction between protein and DNA. Concentrations of around 1 μM ATP appeared to slightly weaken the binding by about 0.7-fold, but that effect goes away with 1 mM nucleotide. Given that neither effect is strong, we interpreted these results as evidence that ZmNDPK1 binds G4 DNA specifically and strongly but not at its active site, perhaps allowing ZmNDPK1 to act as a kinase even in the G4-bound state.

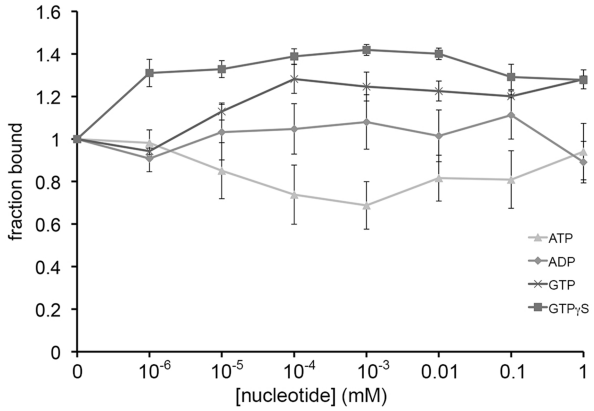

Figure 5. Nucleotides do not inhibit equilibrium ZmNDPK binding. ZmNDPK1 was mixed with folded *hex4*_A5U and increasing concentrations of (▲) ATP, (♦) ADP, (×) GTP, and (■) GTPγS before *hex4*_A5U retention on nitrocellulose was measured. For each, even at 1 mM nucleotide, ZmNDPK1 still strongly binds *hex4*_A5U.

Given the presence of the conserved active site histidine (His115, Figure 1A), we predicted that ZmNDPK1 would be an active nucleoside diphosphate kinase, allowing for additional examination of the relationship between kinase and G4-binding activities. Indeed, ZmNDPK1 is an active kinase, although its specific activity is 50% lower than that of NM23-H2 when the kinase assay is performed in 20 mM KCl or 20 mM LiCl (Figure 6). When the same kinase assays were performed in the presence of prefolded (in KCl) or unfolded (LiCl) G4 motif oligonucleotides, we found that neither the maize nor human NDPK enzymatic activities were substantially altered (Figure 6). These observations, like those from the G4-binding assays in the presence of excess nucleotides (Figure 5), support a model in which G4 DNA does not bind at the active site of NDPKs from maize or human.

To further test the hypothesis that the intact active site is not required for G4 binding by ZmNDPK1, we produced and tested the H115A active site point variant for both its kinase activity and ZmNDPK1 binding. Under standard salt conditions (100 mM KCl), the wild-type ZmNDPK1 has a standard activity of 384 ± 5 units/mg. As expected from previous observations with NM23-H2,[64,65] ZmNDPK1 has no measurable activity for phosphate transfer without its catalytic histidine (11 ± 12 units/mg). We then calculated that H115A binds to prefolded *hex4*_A5U G4 DNA (KCl) with an apparent K_d of 6.9 ± 0.7 and to unfolded *hex4*_A5U G4 DNA (LiCl) with an apparent K_d of 287 ± 14, akin to wild-type binding (Figure 7A,B and Table 2). These results further establish the independence of kinase and G4-DNA binding activities in ZmNDPK1.

Lys149 Is Important for G4 Binding. To test the hypothesis that the divergent C-terminus, which contributes to the unique charged surface of ZmNDPK1, is important for G4 DNA binding, we generated the K149A point variant and tested it for *hex4*_A5U binding. The kinase activity of the K149A variant is not affected, and it has a specific activity in 100 mM KCl of 485 ± 31 units/mg, but *hex4*_A5U G4 DNA binding in KCl was reduced by about 5-fold to 31 ± 2 (Figure 7C and Table 2). Binding of the K149A variant to unfolded *hex4*_A5U G4 DNA in LiCl was essentially abrogated such that even at 2

DOI: 10.1021/bi501284g
Biochemistry 2015, 54, 1743−1757

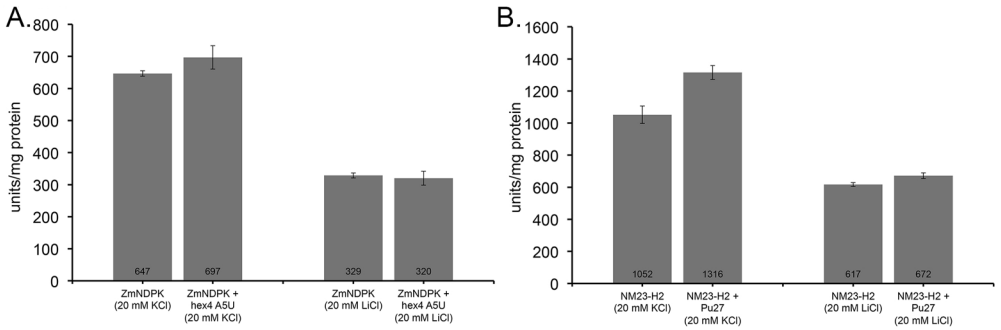

Figure 6. G4 binding does not affect NDPK activity, where one unit is defined as μmol/min·mg. (A) ZmNDPK1 activity is not affected significantly by the presence of folded or unfolded *hex4*_A5U DNA in KCl or LiCl. (B) NMH23-H2 is activity is not affected significantly by the presence of folded or unfolded Pu27 DNA in KCl or LiCl.

μM protein (20 000-fold excess protein over oligonucleotide) binding to the nitrocellulose membrane had not saturated (Table 2).

ZmNDPK1 Binds to Folded G4 DNA. Finally, we used FRET fluorescence spectroscopy to determine if ZmNDPK1 binds to folded or to unfolded G4 DNA. We performed binding titrations using FRET-labeled G4 probes, either *hex4*_A5U or Pu27, against either ZmNDPK1 or NM23-H2 in KCl or LiCl. Interaction between the 5′ and 3′ end of the oligonucleotide is measured by an increase in FRET acceptor emission (TAMRA at 585 nm), after excitation of the donor (6-FAM at 475 nm). When the oligonucleotide 5′ and 3′ ends are far apart, as they are in unfolded single-stranded G-rich DNA, FRET is not detected. When the oligonucleotide 5′ and 3′ ends are close, as in the G4 folded state, FRET signals are measured. An increase in acceptor emission relative to the total donor and acceptor emission is measured by P_F (eq 2). P_F is close to 1 if the FRET probes are independent and the value decreases with increasing FRET. If NDPK were to stabilize the unfolded form of the quadruplex-forming motif, we predicted that protein binding would diminish FRET and that P_F would increase with protein titration. If NDPK were to stabilize the folded form of the quadruplex-forming motif, then we predicted that protein binding would increase FRET and that P_F would decrease with protein titration. No change in P_F would occur without the presence of both the donor and acceptor fluorophores.

ZmNDPK1 mixed with FRET-labeled *hex4*_A5U and NM23-H2 mixed with FRET-labeled Pu27 both resulted in increased FRET in G4s that were prefolded with KCl (Figure 8A,B). FRET increase was visualized by normalizing the emission spectra to the donor emission peak at 520 nm and measured by changes in P_F of −0.07 ± 0.02 for ZmNDPK1/*hex4*_A5U and −0.03 ± 0.02 for NM23-H2/Pu27 (Figure 8 and Table 3). By *t* test analysis, these changes in P_F show statistical relevance at *P*-values <0.05 (Table 3). Moreover, both proteins induced strong FRET when mixed with oligonucleotides that were not prefolded but were in LiCl-containing buffers (Figure 8C,D). Specifically, when ZmNDPK1 was mixed with *hex4*_A5U that was not prefolded, P_F changed by −0.17 ± 0.03 and when NM23-H2 was mixed with Pu27 that was not prefolded, P_F changed by −0.08 ± 0.01 (Table 3). *t* tests also show *P*-values <0.05 for these changes with protein titration. Importantly, *t* test analysis shows statistical significance for the stronger effect of mixing protein with oligonucleotides that were annealed in LiCl relative to mixing protein with oligonucleotides that were prefolded in KCl (Table 3). Similar behavior was seen when the proteins were mixed with their noncognate pairs (Figure 8E−H and Table 3). No combination of protein with single-labeled oligonucleotide (FAM or TAMRA alone) caused FRET emission at 585 nm when illuminated at 475 nm (Figure S8), confirming that the measured FRET signals were dependent on the double-labeled oligonucleotides. No combination of protein with FRET-labeled oligonucleotide caused a decrease in FRET or coupled increase in P_F (Table 3), indicating all combinations of protein, oligonucleotide, and salt resulted in a bound G4 oligonucleotide conformation.

DISCUSSION

G4s in Maize. Maize is a staple crop across the globe as a source of nutrition and energy that fuels economic development. Additionally, maize is a historic, model genetic organism for studying fundamental mechanisms of eukaryotic genome composition.[66] For example, transposable DNA elements,[67] and the capping properties that characterize telomere function[68] are among the historic discoveries in maize. Interestingly, G4 motifs are clustered in known regulatory regions of some genes, in particular those that are involved in stress response metabolic pathways in maize.[11] Interestingly, in *E. coli*, antisense G4 motifs found at promoter regions decrease gene expression whereas antisense G4 motifs found in 5′UTRs increase gene expression,[13] suggesting that differences in G4 position relative to transcription start sites might have functional consequences in the cell. As such, understanding the fundamental mechanisms of G4 binding proteins in maize, a model grass species with a large and complex genome, affords new opportunities to advance understanding of G4 biology while gaining information that could be useful for crop improvement.

G4 motifs are found distributed throughout the maize genome, as they are in the human genome,[8] but in maize they are more likely found within the transcribed gene than in upstream promoter regions.[11] Given the functional significance of a G4 motif in regulating *c-myc* gene expression, we predict that the positioning of the G4 motif within the 5′UTR of maize genes may also represent a similarly broad, conserved mechanism for transcriptional regulation. In fact, our discovery that ZmNDPK1 binds to *hex4*_A5U bolsters this prediction and suggests that G4 binding by NDPKs may represent an ancient and conserved regulatory mechanism in plants and animals.

Binding Mode of G4 to NDPK. We propose that each hexamer of ZmNDPK1 or NM23-H2 binds tightly and cooperatively to two G-rich oligonucleotides and stabilize a

DOI: 10.1021/bi501284g
Biochemistry 2015, 54, 1743−1757

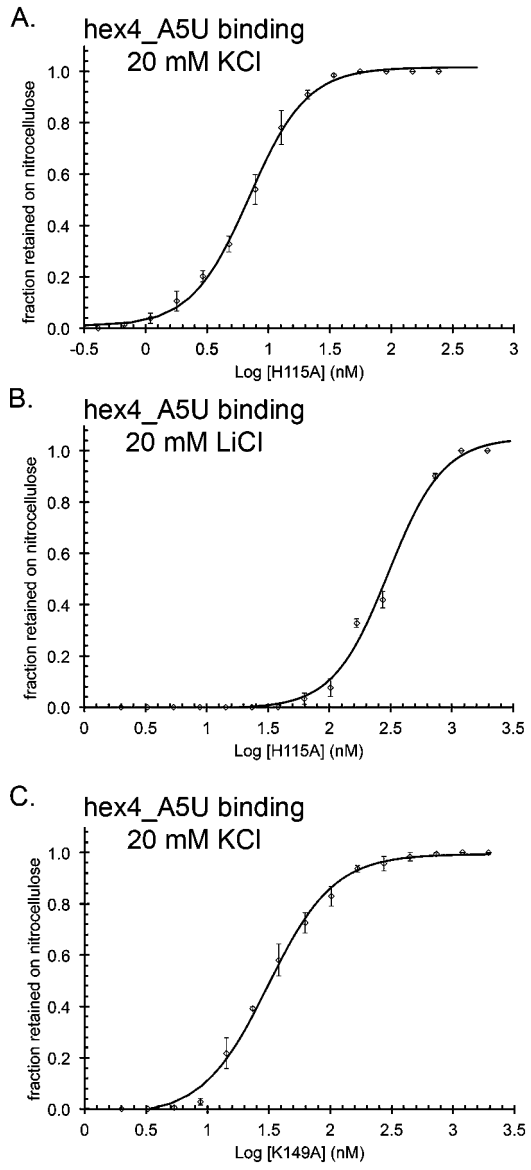

Figure 7. Point variants of ZmNDPK1 show different DNA binding activities. (A) Increasing H115A (active site) variant ZmNDPK1 concentration increases the fraction of *hex4*_A5U G4 oligonucleotide that is retained on the nitrocellulose in 20 mM KCl. The H115A variant binds to prefolded *hex4*_A5U DNA in KCl with about the same affinity as wild-type ZmNDPK1. (B) Increasing H115A (active site) variant ZmNDPK1 concentration increases the fraction of *hex4*_A5U G4 oligonucleotide that is retained on the nitrocellulose in 20 mM LiCl. The H115A variant binds to unfolded *hex4*_A5U DNA in LiCl with about the same affinity as wild-type ZmNDPK1. (C) Increasing K149A (C-terminal) variant ZmNDPK1 concentration increases the fraction of *hex4*_A5U G4 oligonucleotide that is retained on the nitrocellulose in 20 mM KCl. The K149A variant binds to prefolded *hex4*_A5U DNA in KCl with 5-fold weaker affinity.

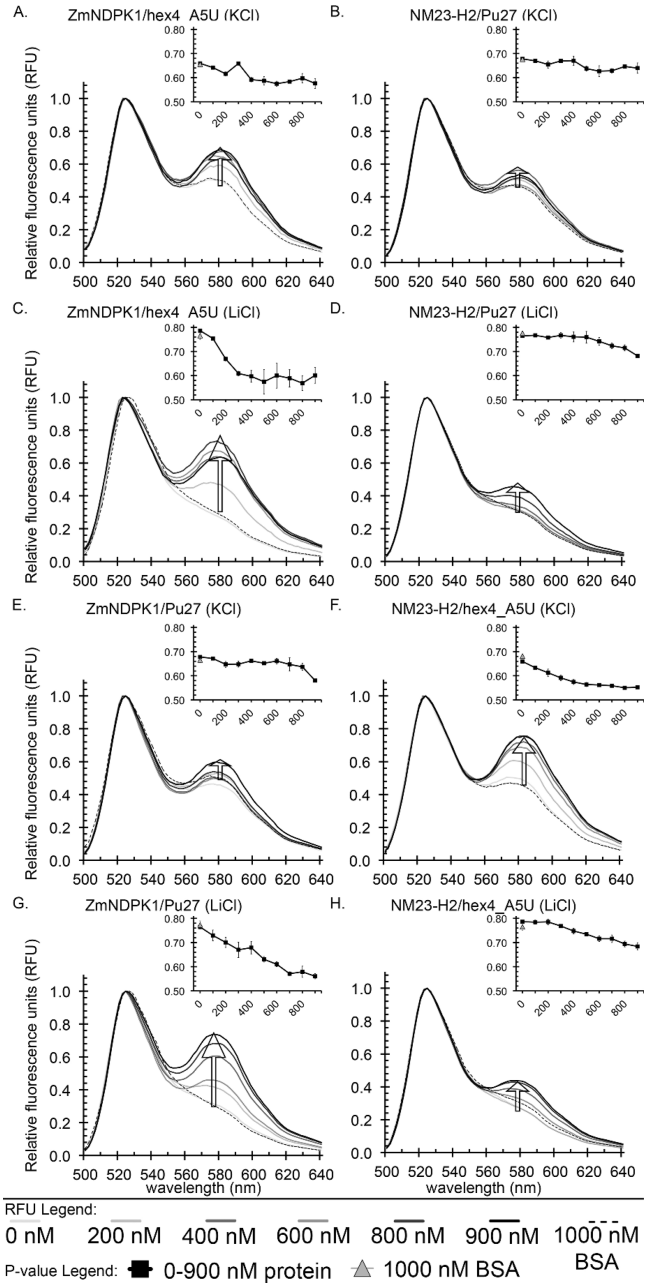

Figure 8. ZmNDPK1 and NM23-H2 both bind to folded G4 DNA, whether prefolded in KCl or not prefolded in LiCl. All spectra are normalized to the 520 nm maximum, for simplicity. All sets of spectra are drawn with increasingly dark lines with increasing protein concentration, showing every-other point in the titration for clarity (the legend is at bottom). A 1000 nM BSA control (dotted line) was performed to show that the increase in FRET is NDPK-specific because the BSA control is identical to the 0 nM NDPK point both in fluorescence spectrum and P_F. Each inset plots P_F as protein concentration in nM on the *x*-axis and P_F on the *y*-axis, showing each point along the titration. (A) ZmNDPK mixed with FRET-labeled prefolded *hex4*_A5U (in KCl) shows a small but significant increase in FRET efficiency at 585 nm with a coupled decrease in P_F (inset) with titrating protein. (B) NM23-H2 mixed with FRET-labeled prefolded Pu27 (in KCl) shows a small but significant increase in FRET efficiency at 585 nm with a coupled decrease in P_F (inset) with titrating protein. (C) ZmNDPK mixed with FRET-labeled unfolded *hex4*_A5U (in LiCl) shows a large and significant increase in FRET efficiency at 585 nm with a coupled decrease in P_F (inset) with titrating protein. (D) NM23-H2 mixed with FRET-labeled unfolded

folded G4 conformation. In the case of a prefolded G-rich oligonucleotide, this model explains both straightforward binding titrations measured by protein/DNA retention on nitrocellulose (Figure 4) and fluorescence experiments that show stabilization of the folded conformation, measured by increased FRET efficiency between the 5′ and 3′ end of FAM/TAMRA labeled oligonucleotides (Figure 8). Mechanistically, the two homologues may bind the G4 somewhat differently because the three amino acids that are implicated in NM23-H2

DOI: 10.1021/bi501284g
Biochemistry 2015, 54, 1743−1757

Figure 8. continued

Pu27 (in LiCl) shows a moderate but significant increase in FRET efficiency at 585 nm with a coupled decrease in P_F (inset) with titrating protein. (E) ZmNDPK mixed with FRET-labeled prefolded Pu27 (in KCl) shows a small but significant increase in FRET efficiency at 585 nm with a coupled decrease in P_F (inset) with titrating protein. (F) NM23-H2 mixed with FRET-labeled prefolded *hex4*_A5U (in KCl) shows a significant increase in FRET efficiency at 585 nm with a coupled decrease in P_F (inset) with titrating protein. (G) ZmNDPK mixed with FRET-labeled unfolded Pu27 (in LiCl) shows a large and significant increase in FRET efficiency at 585 nm with a coupled decrease in P_F (inset) with titrating protein. (H) NM23-H2 mixed with FRET-labeled unfolded *hex4*_A5U (in KCl) shows a significant increase in FRET efficiency at 585 nm with a coupled decrease in P_F (inset) with titrating protein.

Table 3

NDPK homologue	oligonuclotide (salt)	ΔP_F	*P*-value (*t* test)	*P*-value salt pair
ZmNDPK1	hex4_A5U (KCl)	−0.07 ± 0.02	0.010	
ZmNDPK1	hex4_A5U (LiCl)	−0.17 ± 0.03	0.006	0.03
NM23-H2	Pu27 (KCl)	−0.03 ± 0.02	0.040	
NM23-H2	Pu27 (LiCl)	−0.08 ± 0.01	0.002	0.02
ZmNDPK1	Pu27 (KCl)	−0.06 ± 0.01	0.006	
ZmNDPK1	Pu27 (LiCl)	−0.20 ± 0.01	0.0007	0.005
NM23-H2	hex4_A5U (KCl)	−0.11 ± 0.01	0.001	
NM23-H2	hex4_A5U (LiCl)	−0.10 ± 0.02	0.004	0.38

DNA binding (Arg34, Asn69, and Lys135)[57] are not conserved in ZmNDPK1 (Figure 1). Nonetheless, this simple model explains our data as concerns NDPK binding to prefolded G4 DNA.

Binding of oligonucleotides that are not prefolded could be explained by two variations of this model. In one variation, NDPK may function as a folding chaperone, binding weakly to a form of the unfolded oligonucleotide that has some features of the G4 but is not tightly folded and, in doing so, stabilizes G4 formation for tight binding. We know from TDS measurements that neither *hex4*_A5U nor Pu27 adopt a folded G4 in LiCl (Figure S1). Nonetheless, the unfolded oligonucleotide is likely a structurally heterogeneous ligand in solution. For example, tandem Gs could transiently form a motif like a Hoogsteen base pair or a looped structure that is recognized by NDPK, and, upon binding, the intramolecular G4 folded conformation would be stabilized. In the other variation, NDPK binds to the single-stranded oligonucleotide that then recruits a second oligonucleotide, inducing an increase in intermolecular FRET. Both model variations are supported by our observation that unfolded single-stranded G-rich DNA binding by either protein results in an increase of FRET efficiency (Figure 8). The first variation is supported by the observation that NM23-H2 appears to bind to Pu27 or *hex4*_A5U in LiCl-containing buffer with about the same affinity as it does in KCl-containing buffer (Figure 4 and Table 2). The second variation is supported by the observation that ZmNDPK1 binds more weakly and with more steep cooperativity to single-stranded G-rich DNA than to G4-folded DNA (Figure 4 and Table 2).

Competition for G4 binding by other variants of the sequence support the idea that ZmNDPK1 has some nonspecific DNA binding activity, but is quite specific for folded G4s like *hex4*_A5U, *hex4*_AUG RNA, and Pu27 (Table 1 and Figure S7). Indeed, other similarly folded G4s would likely interact with ZmNDPK1 with high affinity but *hex4*_A5I does not compete well for binding, indicating the binding includes some degree of specificity for particular G4 structures, and not a generic structural feature common to different G4s (Table 1 and Figure S7). Importantly, under no condition that we tested did either NDPK homologue support unfolding of the G4 or stabilization of the unfolded conformation (Figure 8). Rather, NDPK appears to function as a stable G4-binding protein, akin to XPB and distinct from other G4-interacting proteins like XPD or Up1 that possess G4 helicase or unfolding activities.[12,25] Our findings further suggest that ZmNDPK1 and NM23-H2 have important biochemical differences in binding single-stranded G-rich DNA (Figures 4 and 8). Additionally, the high affinity of NM23-H2 for prefolded G4s (Figures 4 and 8) raises questions about the proposed model in which NM23-H2 functions in stabilizing single-stranded G-rich DNA.[53,62,69]

Structural Basis for G4 Binding by NDPKs. Given the sequence and structural similarities between NDPK homologues (Figures 1 and 2), the difference between binding modes of these two eukaryotic proteins for single-stranded G-rich DNA is surprising. The only tertiary structural differences between the maize and human proteins lies in the apparent flexibility of the sequence divergent active site loop that, in ZmNDPK1 moderates further oligomerization of the hexamer (Figures 1, 2, and S5). Despite otherwise high homology, however, additional differences in the C-terminus are sufficient to generate a homologue-specific antibody and might explain the altered behavior (Figures 1, 2 and S2). The divergent C-terminus is far from the active site, clustered at the edge between the trimer and dimer faces of the protein and contributing strong basic patches that are specific to the maize homologue (Figure 2). Neither an open nor functional active site is required for G4 binding (Figures 5A and B, 6, and 7), supporting the idea that this far-away region could be important. Similarly, PA, the adenine-rich oligonucleotide with interspersed *G*'s, does not compete for G4 binding (Table 1 and Figure S7B) as it would if an oligonucleotide bound with sequential *G*'s in three active sites of a trimer as previously proposed.[53]

From these observations, we predicted that nucleic acids bind to ZmNDPK1 at the basic patches located at the edge of the trimer−dimer interface, centered at the C-terminal most Lys149 (Figures 1 and 2). Interestingly, NM23-H2 lacks such a C-terminal basic residue, ending instead at a conserved glutamate (NM23-H2 Glu152 or ZmNDPK1 Glu148), raising the possibility that ZmNDPK1 Lys149 may contribute to the recruitment of single-stranded G-rich DNA. In fact, altering Lys149 to an alanine (K149A) reduces prefolded *hex4*_A5U G4 binding by about 5-fold, interestingly to the same level that NM23-H2 binds to the same prefolded oligonucleotide (Figures 4 and 7 and Table 2). The K149A point variant is deficient in binding to *hex4*_A5U when it is not prefolded into G4 (Table 2). Clearly, this single amino acid defines a unique property of the plant NDPK homologue that we discovered.

Indeed, the effect of the terminal lysine on G4-binding properties may have important biological implications because of its distinct phylogenetic distribution within some of the grass species within the plant kingdom (Figure S4). Most plant species encode one or more small NDPKs (~150 aa in length), but the ZmNDKP1-type (identified as the "YEK" group in Figure S4) appears to be a derived variant found in members of the panicoid group of the *Poaceae* family, not limited to maize. Plant species with this YEK-type NDPK include maize,

DOI: 10.1021/bi501284g
Biochemistry 2015, 54, 1743−1757

sorghum, sugar cane, fox tail millet, and switchgrass, some of the worlds leading food, feed, and biofuel producing grass species. That these species have maintained this specific amino acid variant despite strong sequence conservation of the protein as a whole, and given the presence of other small NDPKs (ZmNDPK2 in the case of maize, Figure S4), suggest that its unique and important properties may be evolutionarily important. We speculate that those properties could play a role in *Poaceae*-species diversification or coevolution with G4 elements in the genomes, an interesting avenue of further investigation.

Implications for *in Vivo* Activity. Given the conservation of G4 structures in prokaryotes and eukaryotes as well as the conservation of G4-compatible telomere repeats in plants and mammals, it is not surprising that plants would use similar genic G4s to modulate genome dynamics. There is no clear functional *c-myc* ortholog in maize that controls the cell cycle,[70] so direct comparisons of biological functions in regard to *myc* activation are limited. Even so, we have discovered intriguing similarities and differences between the two homologues that may illuminate a range of function attributed to NDPK/G4 interactions at different genic locations in a species-specific way.

NM23-H2 binds both folded and unfolded G4s with similar affinities and in a manner that promotes close contact of the 5′ and 3′ ends of the oligonucleotide, presumably by stabilizing a folded G4 conformation, together suggesting the protein binds both ligands in a similar conformation (Figures 4 and 8). NM23-H2 binds this nuclease sensitive region of DNA, whether prefolded or not, that is far upstream from the *c-myc* promoter, enhancing c-myc expression.[14]

In contrast, the *hex4*_A5U G-rich region we used as a probe for ZmNDPK1 binding is found just downstream of the transcription start site, within the 5′UTR of *hexokinase4*, a region of DNA that must be opened for transcription to occur. ZmNDPK1 binds more weakly to single-stranded G-rich DNA than it does to folded G4, but then stabilizes a folded form of the G4, whether inter- or intramolecular (Figures 4 and 8). It is possible that ZmNDPK1 stabilizes intramolecular G4s from the template DNA strand or intermolecular-type G4s from adjacent motifs, sister chromatids, or transcripts. Given the prominence of G4 motifs in the antisense strand of 5′-UTRs of maize genes,[11] it is also possible that NDPK could impact nascent RNA formation or progression of the transcription bubble. Similar overrepresentation of AUG G4 motifs at start codons in the sense strand of maize genes[11] suggests that interaction of ZmNDPK1 with an RNA motif on the nascent transcript might also have downstream implications for translation. Alternatively, an A5U-type G4 element could contribute to RNA polymerase pausing or blocking, while localizing active NDPK to maintain a high ribonucleotide triphosphate pool. Indeed, NM23-H2 was recently shown to tether to the C-terminal domain of dynamin to increase GTP pools at membranes, so there is precedent for the targeted localization of NDPK enzymatic activity via interaction with another molecule.[35] Certainly the mechanisms by which NM23-H2 exerts control over c-myc or ZmNDPK1 over genes like *hexokinase4* are likely complex, given the multifactorial and dynamic interactions between DNA isoforms, transcription factors and chromatin proteins. Our study shows that not all aspects of NDPK function translate across taxonomic boundaries and that such comparative analyses will continue to shed light on the biologically relevant mechanism of NDPK DNA binding activities.

Conclusions. In conclusion, we have characterized the first plant G4-binding protein, which was discovered through a ligand-binding screen of a cDNA expression library. This G4 binding protein is a nucleoside diphosphate kinase, akin to human NM23-H2. Biochemical experiments confirmed the specificity of ZmNDPK1 for G4 structures and identified differences in the binding properties of human and maize NDPK homologues to single-stranded, G-rich DNA sequences that are not prefolded into G4 structures, highlighting potentially different biological roles of these NDPKs.

■ ASSOCIATED CONTENT

Supporting Information

Supporting Information includes additional figures and methods. This material is available free of charge via the Internet at http://pubs.acs.org.

Accession Codes

The coordinates for ZmNDPK1 have been deposited in the PDB with PDB ID 1VYA. The sequence of the full-length cDNA was deposited to NCBI as GenBank Accession number KM347972.

■ AUTHOR INFORMATION

Corresponding Author

*Phone: (850) 645-9318. E-mail: mestroupe@bio.fsu.edu.

Funding

This work was supported by National Science Foundation award MCB1149763 to M.E.S. and Florida State University Council on Research and Creativity Planning Grant awards to M.E.S. (OMNI-0000035907) and H.W.B. (OMNI-0000025471).

Notes

The authors declare no competing financial interest.

■ ACKNOWLEDGMENTS

We thank Dr. Brian Miller, Dr. Hong Li, Dr. Christopher Stroupe, and Joseph Pennington for useful discussions; Dr. Michael Zawronty for help with Python; and Dr. David Gilbert for use of his laboratory's slot blot apparatus.

■ ABBREVIATIONS:

A5U, antisense 5′ UTR; aa, amino acid; ADP, adenosine diphosphate; ATP, adenosine triphosphate; cDNA, complementary DNA; CN/DAB, chloronaphthol/diaminobenzidine; DNA, DNA; DTT, dithiothreitol; dsDNA, double-stranded DNA; EDTA, ethylenediaminetetraacetic acid; FRET, Förster resonance energy transfer; G4, G-quadruplex; GTP, guanosine triphosphate; GTPγS, guanosine 5′-*O*-[gamma-thio]-triphosphate; HRP, horseradish peroxidase; LTR, long terminal repeat; NADH, reduced form of β-NAD; NDPK, nucleoside diphosphate kinase; NM23, nonmetastatic 23; PEG, polyethylene glycol; PMSF, phenylmethanesulfonyl fluoride; RNA, ribonucleic acid; ssDNA, single-stranded DNA; TBS, Tris-buffered saline; TBST, Tris-buffered saline with Tween 20; TDS, thermal difference spectrum; TTP, thymidine triphosphate; UTR, untranslated region; XPB, xeroderma pigmentosum B; XPD, xeroderma pigmentosum D; Zm, *Zea mays*; β-NAD, β-nicotinamide adenine dinucleotide

DOI: 10.1021/bi501284g
Biochemistry 2015, 54, 1743−1757

REFERENCES

(1) Huppert, J. L. (2008) Four-stranded nucleic acids: structure, function and targeting of G-quadruplexes. *Chem. Soc. Rev. 37*, 1375−1384.

(2) Burge, S., Parkinson, G. N., Hazel, P., Todd, A. K., and Neidle, S. (2006) Quadruplex DNA: sequence, topology and structure. *Nucleic Acids Res. 34*, 5402−5415.

(3) Zhang, S., Wu, Y., and Zhang, W. (2014) G-quadruplex structures and their interaction diversity with ligands. *ChemMedChem 9*, 899−911.

(4) Juranek, S. A., and Paeschke, K. (2012) Cell cycle regulation of G-quadruplex DNA structures at telomeres. *Curr. Pharm. Des. 18*, 1867−1872.

(5) Lipps, H. J., and Rhodes, D. (2009) G-quadruplex structures: in vivo evidence and function. *Trends Cell Biol. 19*, 414−422.

(6) Mullen, M. A., Olson, K. J., Dallaire, P., Major, F., Assmann, S. M., and Bevilacqua, P. C. (2010) RNA G-Quadruplexes in the model plant species *Arabidopsis thaliana*: prevalence and possible functional roles. *Nucleic Acids Res. 38*, 8149−8163.

(7) Maizels, N., and Gray, L. T. (2013) The G4 genome. *PLoS Genet. 9*, e1003468.

(8) Huppert, J. L., and Balasubramanian, S. (2007) G-quadruplexes in promoters throughout the human genome. *Nucleic Acids Res. 35*, 406−413.

(9) Lexa, M., Kejnovsky, E., Steflova, P., Konvalinova, H., Vorlickova, M., and Vyskot, B. (2014) Quadruplex-forming sequences occupy discrete regions inside plant LTR retrotransposons. *Nucleic Acids Res. 42*, 968−978.

(10) Murat, P., and Balasubramanian, S. (2014) Existence and consequences of G-quadruplex structures in DNA. *Curr. Opin. Genet. Dev. 25C*, 22−29.

(11) Andorf, C. M., Kopylov, M., Dobbs, D., Koch, K. E., Stroupe, M. E., Lawrence, C. J., and Bass, H. W. (2014) G-Quadruplex (G4) Motifs in the Maize (*Zea mays* L.) Genome Are Enriched at Specific Locations in Thousands of Genes Coupled to Energy Status, Hypoxia, Low Sugar, and Nutrient Deprivation. *J. Genet. Genomics 41*, 627−647.

(12) Gray, L. T., Vallur, A. C., Eddy, J., and Maizels, N. (2014) G quadruplexes are genomewide targets of transcriptional helicases XPB and XPD. *Nat. Chem. Biol. 10*, 313−318.

(13) Holder, I. T., and Hartig, J. S. (2014) A Matter of Location: Influence of G-Quadruplexes on *Escherichia coli* Gene Expression. *Chem. Biol. 21*, 1511−1521.

(14) Siddiqui-Jain, A., Grand, C. L., Bearss, D. J., and Hurley, L. H. (2002) Direct evidence for a G-quadruplex in a promoter region and its targeting with a small molecule to repress c-MYC transcription. *Proc. Natl. Acad. Sci. U.S.A. 99*, 11593−11598.

(15) Lam, E. Y., Beraldi, D., Tannahill, D., and Balasubramanian, S. (2013) G-quadruplex structures are stable and detectable in human genomic DNA. *Nat. Commun. 4*, 1796.

(16) Bochman, M. L., Paeschke, K., and Zakian, V. A. (2012) DNA secondary structures: stability and function of G-quadruplex structures. *Nat. Rev. Genet. 13*, 770−780.

(17) Shen, Y., Kim, J. I., and Song, P. S. (2005) NDPK2 as a signal transducer in the phytochrome-mediated light signaling. *J. Biol. Chem. 280*, 5740−5749.

(18) Lane, A. N., Chaires, J. B., Gray, R. D., and Trent, J. O. (2008) Stability and kinetics of G-quadruplex structures. *Nucleic Acids Res. 36*, 5482−5515.

(19) Biffi, G., Tannahill, D., McCafferty, J., and Balasubramanian, S. (2013) Quantitative visualization of DNA G-quadruplex structures in human cells. *Nat. Chem. 5*, 182−186.

(20) Henderson, A., Wu, Y., Huang, Y. C., Chavez, E. A., Platt, J., Johnson, F. B., Brosh, R. M., Jr., Sen, D., and Lansdorp, P. M. (2014) Detection of G-quadruplex DNA in mammalian cells. *Nucleic Acids Res. 42*, 860−869.

(21) Hwang, H., Kreig, A., Calvert, J., Lormand, J., Kwon, Y., Daley, J. M., Sung, P., Opresko, P. L., and Myong, S. (2014) Telomeric Overhang Length Determines Structural Dynamics and Accessibility to Telomerase and ALT-Associated Proteins. *Structure 22*, 842−853.

(22) Ray, S., Bandaria, J. N., Qureshi, M. H., Yildiz, A., and Balci, H. (2014) G-quadruplex formation in telomeres enhances POT1/TPP1 protection against RPA binding. *Proc. Natl. Acad. Sci. U.S.A. 111*, 2990−2995.

(23) Paeschke, K., Simonsson, T., Postberg, J., Rhodes, D., and Lipps, H. J. (2005) Telomere end-binding proteins control the formation of G-quadruplex DNA structures in vivo. *Nat. Struct. Mol. Biol. 12*, 847−854.

(24) Postel, E. H., Mango, S. E., and Flint, S. J. (1989) A nuclease-hypersensitive element of the human c-myc promoter interacts with a transcription initiation factor. *Mol. Cell. Biol. 9*, 5123−5133.

(25) Cogoi, S., Paramasivam, M., Spolaore, B., and Xodo, L. E. (2008) Structural polymorphism within a regulatory element of the human KRAS promoter: formation of G4-DNA recognized by nuclear proteins. *Nucleic Acids Res. 36*, 3765−3780.

(26) Giraldo, R., Suzuki, M., Chapman, L., and Rhodes, D. (1994) Promotion of parallel DNA quadruplexes by a yeast telomere binding protein: a circular dichroism study. *Proc. Natl. Acad. Sci. U.S.A. 91*, 7658−7662.

(27) Postel, E. H., Berberich, S. J., Flint, S. J., and Ferrone, C. A. (1993) Human c-myc transcription factor PuF identified as nm23-H2 nucleoside diphosphate kinase, a candidate suppressor of tumor metastasis. *Science 261*, 478−480.

(28) Bilitou, A., Watson, J., Gartner, A., and Ohnuma, S. (2009) The NM23 family in development. *Mol. Cell. Biochem. 329*, 17−33.

(29) Garces, E., and Cleland, W. W. (1969) Kinetic studies of yeast nucleoside diphosphate kinase. *Biochemistry 8*, 633−640.

(30) Postel, E. H. (2003) Multiple biochemical activities of NM23/NDP kinase in gene regulation. *J. Bioenerg. Biomembr. 35*, 31−40.

(31) Morin-Leisk, J., and Lee, T. H. (2008) Nucleotide-dependent self-assembly of nucleoside diphosphate kinase (NDPK) in vitro. *Biochim. Biophys. Acta 1784*, 2045−2051.

(32) Freije, J. M., Blay, P., MacDonald, N. J., Manrow, R. E., and Steeg, P. S. (1997) Site-directed mutation of Nm23-H1. Mutations lacking motility suppressive capacity upon transfection are deficient in histidine-dependent protein phosphotransferase pathways in vitro. *J. Biol. Chem. 272*, 5525−5532.

(33) Shen, Y., Han, Y. J., Kim, J. I., and Song, P. S. (2008) Arabidopsis nucleoside diphosphate kinase-2 as a plant GTPase activating protein. *BMB Rep. 41*, 645−650.

(34) Francois-Moutal, L., Maniti, O., Marcillat, O., and Granjon, T. (2013) New insights into lipid-nucleoside diphosphate kinase-D interaction mechanism: protein structural changes and membrane reorganisation. *Biochim. Biophys. Acta 1828*, 906−915.

(35) Boissan, M., Montagnac, G., Shen, Q., Griparic, L., Guitton, J., Romao, M., Sauvonnet, N., Lagache, T., Lascu, I., Raposo, G., Desbourdes, C., Schlattner, U., Lacombe, M. L., Polo, S., van der Bliek, A. M., Roux, A., and Chavrier, P. (2014) Membrane trafficking. Nucleoside diphosphate kinases fuel dynamin superfamily proteins with GTP for membrane remodeling. *Science 344*, 1510−1515.

(36) Lombardi, D., Lacombe, M. L., and Paggi, M. G. (2000) nm23: unraveling its biological function in cell differentiation. *J. Cell. Physiol. 182*, 144−149.

(37) Finan, P. M., White, I. R., Redpath, S. H., Findlay, J. B., and Millner, P. A. (1994) Molecular cloning, sequence determination and heterologous expression of nucleoside diphosphate kinase from Pisum sativum. *Plant Mol. Biol. 25*, 59−67.

(38) Dorion, S., Matton, D. P., and Rivoal, J. (2006) Characterization of a cytosolic nucleoside diphosphate kinase associated with cell division and growth in potato. *Planta 224*, 108−124.

(39) Nomura, T., Yatsunami, K., Honda, A., Sugimoto, Y., Fukui, T., Zhang, J., Yamamoto, J., and Ichikawa, A. (1992) The amino acid sequence of nucleoside diphosphate kinase I from spinach leaves, as deduced from the cDNA sequence. *Arch. Biochem. Biophys. 297*, 42−45.

(40) Dancer, J., Neuhaus, H. E., and Stitt, M. (1990) Subcellular compartmentation of uridine nucleotides and nucleoside-5′ -diphosphate kinase in leaves. *Plant Physiol. 92*, 637−641.

DOI: 10.1021/bi501284g
Biochemistry 2015, 54, 1743−1757

(41) Kim, Y. H., Kim, M. D., Choi, Y. I., Park, S. C., Yun, D. J., Noh, E. W., Lee, H. S., and Kwak, S. S. (2011) Transgenic poplar expressing Arabidopsis NDPK2 enhances growth as well as oxidative stress tolerance. *Plant Biotechnol. J. 9*, 334−347.
(42) Kim, Y. H., Lim, S., Yang, K. S., Kim, C. Y., Kwon, S. Y., Lee, H. S., Wang, X., Zhou, Z., Ma, D., Yun, D. J., and Kwak, S. S. (2009) Expression of *Arabidopsis NDPK2* increases antioxidant enzyme activites and enhances tolerance to multiple environmental stresses in transgenic sweetpotato plants. *Mol. Breeding 24*, 233−244.
(43) Wang, Z., Li, H., Ke, Q., Jeong, J. C., Lee, H. S., Xu, B., Deng, X. P., Lim, Y. P., and Kwak, S. S. (2014) Transgenic alfalfa plants expressing AtNDPK2 exhibit increased growth and tolerance to abiotic stresses. *Plant Physiol. Biochem. 84C*, 67−77.
(44) Singh, H., LeBowitz, J. H., Baldwin, A. S., Jr., and Sharp, P. A. (1988) Molecular cloning of an enhancer binding protein: isolation by screening of an expression library with a recognition site DNA. *Cell 52*, 415−423.
(45) Otwinowski, Z., and Minor, W. (1997) Processing of X-ray Diffraction Data Collected in Oscillation Mode, In *Methods in Enzymology: Macromolecular Crystallography, Part A* (Carter, C., Jr., Sweet, R., Eds.), pp 307−326, Academic Press, New York.
(46) Adams, P. D., Afonine, P. V., Bunkoczi, G., Chen, V. B., Davis, I. W., Echols, N., Headd, J. J., Hung, L. W., Kapral, G. J., Grosse-Kunstleve, R. W., McCoy, A. J., Moriarty, N. W., Oeffner, R., Read, R. J., Richardson, D. C., Richardson, J. S., Terwilliger, T. C., and Zwart, P. H. (2010) PHENIX: a comprehensive Python-based system for macromolecular structure solution. *Acta Crystallogr. Sect. D, Biol. Crystallogr. 66*, 213−221.
(47) Im, Y. J., Kim, J. I., Shen, Y., Na, Y., Han, Y. J., Kim, S. H., Song, P. S., and Eom, S. H. (2004) Structural analysis of Arabidopsis thaliana nucleoside diphosphate kinase-2 for phytochrome-mediated light signaling. *J. Mol. Biol. 343*, 659−670.
(48) Ryder, S. P., Recht, M. I., and Williamson, J. R. (2008) Quantitative analysis of protein-RNA interactions by gel mobility shift. *Methods Mol. Biol. 488*, 99−115.
(49) Woodbury, C. P., Jr., and von Hippel, P. H. (1983) On the determination of deoxyribonucleic acid-protein interaction parameters using the nitrocellulose filter-binding assay. *Biochemistry 22*, 4730−4737.
(50) Czerwinski, J. D., Hovan, S. C., and Mascotti, D. P. (2005) Quantitative nonisotopic nitrocellulose filter binding assays: bacterial manganese superoxide dismutase-DNA interactions. *Anal. Biochem. 336*, 300−304.
(51) Thomas, P. S. (1980) Hybridization of denatured RNA and small DNA fragments transferred to nitrocellulose. *Proc. Natl. Acad. Sci. U.S.A. 77*, 5201−5205.
(52) Schneider, C. A., Rasband, W. S., and Eliceiri, K. W. (2012) NIH Image to ImageJ: 25 years of image analysis. *Nat. Methods 9*, 671−675.
(53) Dexheimer, T. S., Carey, S. S., Zuohe, S., Gokhale, V. M., Hu, X., Murata, L. B., Maes, E. M., Weichsel, A., Sun, D., Meuillet, E. J., Montfort, W. R., and Hurley, L. H. (2009) NM23-H2 may play an indirect role in transcriptional activation of c-myc gene expression but does not cleave the nuclease hypersensitive element III(1). *Molecular Cancer Ther. 8*, 1363−1377.
(54) Bergmeyer, H. U., Ed. (1974) *Methods of Enzymatic Analysis*, Vol. *II*, Academic Press, Inc, New York and London.
(55) Salas, T. R., Petruseva, I., Lavrik, O., Bourdoncle, A., Mergny, J. L., Favre, A., and Saintome, C. (2006) Human replication protein A unfolds telomeric G-quadruplexes. *Nucleic Acids Res. 34*, 4857−4865.
(56) Sekhon, R. S., Lin, H., Childs, K. L., Hansey, C. N., Buell, C. R., de Leon, N., and Kaeppler, S. M. (2011) Genome-wide atlas of transcription during maize development. *Plant J. 66*, 553−563.
(57) Postel, E. H., Weiss, V. H., Beneken, J., and Kirtane, A. (1996) Mutational analysis of NM23-H2/NDP kinase identifies the structural domains critical to recognition of a c-myc regulatory element. *Proc. Natl. Acad. Sci. U.S.A. 93*, 6892−6897.
(58) Arora, A., and Maiti, S. (2009) Differential biophysical behavior of human telomeric RNA and DNA quadruplex. *J. Phys. Chem. B 113*, 10515−10520.
(59) Joachimi, A., Benz, A., and Hartig, J. S. (2009) A comparison of DNA and RNA quadruplex structures and stabilities. *Bioorg. Med. Chem. 17*, 6811−6815.
(60) Sacca, B., Lacroix, L., and Mergny, J. L. (2005) The effect of chemical modifications on the thermal stability of different G-quadruplex-forming oligonucleotides. *Nucleic Acids Res. 33*, 1182−1192.
(61) Zhang, D. H., Fujimoto, T., Saxena, S., Yu, H. Q., Miyoshi, D., and Sugimoto, N. (2010) Monomorphic RNA G-quadruplex and polymorphic DNA G-quadruplex structures responding to cellular environmental factors. *Biochemistry 49*, 4554−4563.
(62) Raveh, S., Vinh, J., Rossier, J., Agou, F., and Veron, M. (2001) Peptidic determinants and structural model of human NDP kinase B (Nm23-H2) bound to single-stranded DNA. *Biochemistry 40*, 5882−5893.
(63) Kandeel, M., and Kitade, Y. (2010) Substrate specificity and nucleotides binding properties of NM23H2/nucleoside diphosphate kinase homolog from Plasmodium falciparum. *J. Bioenerg. Biomembr. 42*, 361−369.
(64) Postel, E. H., Abramczyk, B. A., Gursky, S. K., and Xu, Y. (2002) Structure-based mutational and functional analysis identify human NM23-H2 as a multifunctional enzyme. *Biochemistry 41*, 6330−6337.
(65) Postel, E. H., and Ferrone, C. A. (1994) Nucleoside diphosphate kinase enzyme activity of NM23-H2/PuF is not required for its DNA binding and in vitro transcriptional functions. *J. Biol. Chem. 269*, 8627−8630.
(66) Schnable, P. S., Ware, D., Fulton, R. S., Stein, J. C., Wei, F., Pasternak, S., Liang, C., Zhang, J., Fulton, L., Graves, T. A., Minx, P., Reily, A. D., Courtney, L., Kruchowski, S. S., Tomlinson, C., Strong, C., Delehaunty, K., Fronick, C., Courtney, B., Rock, S. M., Belter, E., Du, F., Kim, K., Abbott, R. M., Cotton, M., Levy, A., Marchetto, P., Ochoa, K., Jackson, S. M., Gillam, B., Chen, W., Yan, L., Higginbotham, J., Cardenas, M., Waligorski, J., Applebaum, E., Phelps, L., Falcone, J., Kanchi, K., Thane, T., Scimone, A., Thane, N., Henke, J., Wang, T., Ruppert, J., Shah, N., Rotter, K., Hodges, J., Ingenthron, E., Cordes, M., Kohlberg, S., Sgro, J., Delgado, B., Mead, K., Chinwalla, A., Leonard, S., Crouse, K., Collura, K., Kudrna, D., Currie, J., He, R., Angelova, A., Rajasekar, S., Mueller, T., Lomeli, R., Scara, G., Ko, A., Delaney, K., Wissotski, M., Lopez, G., Campos, D., Braidotti, M., Ashley, E., Golser, W., Kim, H., Lee, S., Lin, J., Dujmic, Z., Kim, W., Talag, J., Zuccolo, A., Fan, C., Sebastian, A., Kramer, M., Spiegel, L., Nascimento, L., Zutavern, T., Miller, B., Ambroise, C., Muller, S., Spooner, W., Narechania, A., Ren, L., Wei, S., Kumari, S., Faga, B., Levy, M. J., McMahan, L., Van Buren, P., Vaughn, M. W., Ying, K., Yeh, C. T., Emrich, S. J., Jia, Y., Kalyanaraman, A., Hsia, A. P., Barbazuk, W. B., Baucom, R. S., Brutnell, T. P., Carpita, N. C., Chaparro, C., Chia, J. M., Deragon, J. M., Estill, J. C., Fu, Y., Jeddeloh, J. A., Han, Y., Lee, H., Li, P., Lisch, D. R., Liu, S., Liu, Z., Nagel, D. H., McCann, M. C., SanMiguel, P., Myers, A. M., Nettleton, D., Nguyen, J., Penning, B. W., Ponnala, L., Schneider, K. L., Schwartz, D. C., Sharma, A., Soderlund, C., Springer, N. M., Sun, Q., Wang, H., Waterman, M., Westerman, R., Wolfgruber, T. K., Yang, L., Yu, Y., Zhang, L., Zhou, S., Zhu, Q., Bennetzen, J. L., Dawe, R. K., Jiang, J., Jiang, N., Presting, G. G., Wessler, S. R., Aluru, S., Martienssen, R. A., Clifton, S. W., McCombie, W. R., Wing, R. A., and Wilson, R. K. (2009) The B73 maize genome: complexity, diversity, and dynamics. *Science 326*, 1112−1115.
(67) McClintock, B. (1930) A Cytological Demonstration of the Location of an Interchange between Two Non-Homologous Chromosomes of Zea Mays. *Proc. Natl. Acad. Sci. U.S.A. 16*, 791−796.
(68) McClintock, B. (1939) The Behavior in Successive Nuclear Divisions of a Chromosome Broken at Meiosis. *Proc. Natl. Acad. Sci. U.S.A. 25*, 405−416.
(69) Thakur, R. K., Kumar, P., Halder, K., Verma, A., Kar, A., Parent, J. L., Basundra, R., Kumar, A., and Chowdhury, S. (2009) Metastases suppressor NM23-H2 interaction with G-quadruplex DNA within c-

DOI: 10.1021/bi501284g
Biochemistry 2015, 54, 1743−1757

MYC promoter nuclease hypersensitive element induces c-MYC expression. *Nucleic Acids Res. 37*, 172−183.
(70) Loulergue, C., Lebrun, M., and Briat, J. F. (1998) Expression cloning in Fe2+ transport defective yeast of a novel maize MYC transcription factor. *Gene 225*, 47−57.
(71) Sievers, F., and Higgins, D. G. (2014) Clustal Omega, accurate alignment of very large numbers of sequences. *Methods Mol. Biol. 1079*, 105−116.
(72) Pettersen, E. F., Goddard, T. D., Huang, C. C., Couch, G. S., Greenblatt, D. M., Meng, E. C., and Ferrin, T. E. (2004) UCSF Chimera–a visualization system for exploratory research and analysis. *J. Comput. Chem. 25*, 1605−1612.

DOI: 10.1021/bi501284g
Biochemistry 2015, 54, 1743−1757